Environmental Engineering and Management Journal

April 2018, Vol.17, No. 4, 925-936
http://www.eemj.icpm.tuiasi.ro/; http://www.eemj.eu

"Gheorghe Asachi" Technical University of Iasi, Romania

PREPARATION AND CHARACTERIZATION OF NANOCOMPOSITE MATERIAL BASED ON TiO_2-Ag FOR ENVIRONMENTAL APPLICATIONS

Catalina Nutescu Duduman[1], Jose Maria Gómez de Salazar y Caso de Los Cobos[2], Maria Harja[1]*, Maria I. Barrena Pérez[2], Consuelo Gómez de Castro[3], Doina Lutic[4], Olga Kotova[5], Igor Cretescu[6]*

[1]"Gheorghe Asachi" Technical University of Iasi, Faculty of Chemical Engineering and Environmental Protection, Chemical Engineering Department, 73 Prof.dr.doc. Dimitrie Mangeron Street, 700050 Iasi, Romania
[2]Complutense University of Madrid, Faculty of Chemical, Department of Materials Science and Metallurgical Engineering Av. Séneca, 2, 28040 Madrid, Spain
[3]Complutense University of Madrid, Faculty of Chemical, Department of Materials and Chemical Engineering, Av. Séneca, 2, 28040 Madrid, Spain
[4]Alexandru Ioan Cuza University of Iasi, Blvd. Carol I No 11, 700506 Iaşi, Romania
[5]Laboratory of Mineral Raw Materials Technology, Institute of Geology, Komi Science Center, Ural Branch of RAS, Syktyvkar, Komi Republic, Russia
[6]"Gheorghe Asachi" Technical University of Iasi, Faculty of Chemical Engineering and Environmental Protection, Department of Environmental Engineering and Management, 73 Prof.dr.doc. Dimitrie Mangeron Street, 700050 Iasi, Romania

Abstract

A simple and efficient method for preparing Ag-doped TiO_2 nanoparticles was successfully developed, by associating the sol-gel method and the impregnation-reduction. While titanium dioxide is one of the most used solids as photocatalyst, silver is particularly interesting for applications in biological and chemical detection and for its antibacterial properties. Moreover, in photocatalysis silver acts as an electron sink and donor in capturing the photogenerated electrons. The structural and morphological properties of the TiO_2-Ag samples were investigated by XRD, SEM, TEM, SAED and EDAX. The crystallinity degree increased by calcination at 650°C and the nature of the phases changed from anatase to a mixture of anatase, rutile and silver in metallic form and silver oxide. The photocatalytic properties of the synthesized product were evaluated in the UV-assisted photodegradation of Rhodamine 6G and Methyl Blue dyes. The photocatalytic performance in dyes decomposition of the doped samples was better than pure TiO_2.

Key words: nanocomposite, photocatalyst, silver, titanium dioxide

Received: May, 2017; Revised final: January, 2018; Accepted: March, 2018; Published in final edited form: April 2018

1. Introduction

Titanium dioxide (TiO_2) is widely used in environmental protection and energy applications (Nakata and Fujishima, 2012). Among the environmental protection applications, the air and water purification systems, sterilization, manufacturing of self-cleaning surfaces, solar energy conversion, photo-electrochemical conversion can be mentioned (Liu and Bi, 2017; Wang et al., 2017). Another interesting and important application of titanium dioxide nanoparticles is its use in

*Author to whom all correspondence should be addressed: e-mail: mharja@tuiasi.ro; Phone: +40 747 909 645; Fax: +40 232 271 311; icre@tuiasi.ro; Phone: +40 741 914 342; Fax: +40 232 271 311

photocatalytic and photoelectrochemical applications, due to its convenient band gap value of 3.2 eV, non-toxic character, chemical and physical stability, high potential of capturing the solar energy and photocatalytic efficiency, low price etc. (Djoki et al., 2012; Ivanova et. al., 2013; Kartal and Turhan, 2017; Liu et al., 2015). The semiconductive properties of TiO_2-based materials make them useful as sensitizers for redox processes activated by light, due to their electronic structure (Chen et al., 2010; Favier et al., 2016; Lutic et al., 2017; Montazerozohori and Hoseinipour, 2017; Tobaldi et al., 2013).

Titanium dioxide exists in many polymorphs, but the most significant are anatase and rutile. These two polymorphs are semiconductors with rather large band gaps (3.23 and 3.02 eV respectively), therefore they can promote photocatalytic reactions in the presence of visible light (Tobaldi et al., 2013).

A convenient strategy to increase the visible light absorption is the incorporation of noble metals nanoparticles in titania (Cheriyan et al., 2017; Ivanova et al., 2013; Kochuveedu and Kim, 2012). Dopants such as Pt, Pd, Au, Ag improve the photocatalytic efficiency of TiO_2, by preventing the recombination of electron-hole pair (He et al., 2013; Sarina et al., 2013; Wei et al., 2013; Yin et al., 2014). Silver is suitable, nontoxic and much cheaper than the other mentioned noble metals, improving the TiO_2 bioactivity especially in water treatments, because of its intrinsic antibacterial activity against different microorganisms (Amin et al., 2009; Lee et al., 2005; Pham and Lee, 2004; Rupa et al., 2007; Liu et al., 2004). TiO_2-Ag and Ag nanoparticles can be relatively easily obtained by the sol-gel method (Behnajady et al., in press), a method widely employed in materials science. The formation of titanium oxide by the sol-gel method involves connecting Ti monomeric species by either oxo (Ti–O–Ti) or hydroxo (Ti–OH–Ti) bridges, generating polymers in solution. This technology allows obtaining a metal oxide matrix with the required characteristics and adding subsequently containing embedded nanoparticles (Galkina et al., 2011; Gomez de Salazar et al., 2016; Nutescu Duduman et al., 2016a, 2016b). Therefore, by the sol-gel method, TiO_2-Ag nanocomposites with easily controlled particle size can be obtained. The performance of TiO_2 in the photocatalytic processes is influenced by different factors: the nature of the phase, the crystallinity degree, the particles morphology and size, the active facet etc. (Hu et al., 2017; Niu et al., 2012; Vajda et al., 2016). Therefore, the preparation of anatase or rutile TiO_2 materials, with targeted properties is still a difficult task.

Organic dyes are widely used in textile industry, plastic, rubber, toys and many other industries. They have a major impact in the environment in generally, especially in wastewater (Ciobanu et al., 2013; Harja et al., 2011; Harja et al., 2016; Mahmoodi et al., 2017). The dyes originated from textile industry are a major source of water contamination, since, on one part, a lot of industries use organic coloring agents resistant to the conventional treatments such as the common biologic conversion (Tian et al., 2014), and, on another part, because the amounts discharged are quite high (Ciobanu et al., 2014; Rusu et al., 2014).

Rhodamine 6 G (R6G) and Methyl Blue (MB) are usual and convenient model compounds for investigating the performance of semiconductive solids involved for their degradation by advanced methods as: chemical and electrochemical procedures, adsorption, ultrafiltration and photocatalytic degradation in the presence of UV or visible light (Bhakya et al., 2015; Lutic and Cretescu, 2016; Lutic et al., 2012), due to their high stability and coloring power even at concentrations of some ppm range.

In this paper we are describing the procedure for obtaining TiO_2-Ag nanocomposites by using an organic titanium salt as oxide precursor and hydrazine as reducing agent for Ag^+ ions to metallic Ag. After the structural characterization, the solids were tested in the UV-assisted photocatalytic degradation of R6G and MB dyes from aqueous solutions simulating wastewaters.

2. Experimental

2.1. Samples preparation

Titanium tetra-isopropoxide (TIP-$C_{12}H_{28}O_4Ti$), Panreac was used as precursor for preparing the TiO_2-based materials. The other chemicals used in the preparation by sol-gel method: silver nitrate ($AgNO_3$), ethanol (C_2H_6O) 98%, and hydrazine (N_2H_4) 98%, all of analytical purity, were purchased from Pancreac. Nitric acid (HNO_3) 65% (w/w) was used as hydrolysis-condensation ratio controlling agent, ammonia solution (NH_4OH) 0.1 M as neutralization agent, and ethanol as solvent. Bidistilled water was used in all preparations employing aqueous media.

TIP was dissolved in ethanol under magnetic stirring, and then nitric acid was added drop wise until a pH value of 1.5 was reached, to induce the controlled hydrolysis of the titanium salt. After 30 minutes, the ammonia solution was added to neutralize the acid and settle the proper pH value (9-10) to initiate the polycondensation of $Ti(OH)_4$ and generate titania nanoparticles. After 2 h of stirring, the procedure of doping the particles with silver was started by adding $AgNO_3$ and ammonia solution, to bring the pH value to 10-11. After 1 h of stirring, the reducing agent was added and the stirring continued for another hour. The solid was recovered by filtration and dried in the oven at 110°C. A portion of this sample was calcined at 650°C. This calcination temperature was chosen in order to generate a convenient anatase/rutile ratio, since their mixture have, due to the easy different position and wideness of the band gap, the property to hinder the fast electron-hole recombination reaction (Atitar et al., 2015; He et al., 2014; Ibrahim et al., 2017).

Table 1. Synthesis conditions and samples labeling for the TiO_2-Ag nanocomposite

Samples	*TIP, g*	*Ethanol, mL*	*HNO_3, mL*	*NH_4OH, mL*	*$AgNO_3$, g*	*Hydrazine, g*	*Calcined*
TiO_2	5.8	10	50	100	-	133	no
S1	5.8	10	50	100	0.418	133	no
S2	5.8	10	50	100	0.418	133	2h

In the meantime, the presence of some dopants induces the easier anatase-rutile transformation, while others inhibit it (Hanaor and Sorell, 2011). The detailed compositions of the synthesis mixtures and the samples labeling are summarized in Table 1.

The samples morphology and chemical elementary composition were determined by Scanning Electron Microscopy (SEM) – Electron Dispersive Analysis by X-ray (EDAX) analysis, on a JEOL 6400 machine with an Oxford Link EDAX microanalyser and Pentafet light sensing with coupled EDSX-max (Oxford Instruments).

The chemical composition was obtained by performing minimum 5 determinations for each sample, in different points, and averaging the individual results, since EDAX analysis provides local concentrations. The transmission electron microscopy (TEM) and Selected Area Electron Diffraction (SAED) images were obtained on a JEOL JEM-2100 apparatus, working at accelerating voltage mode at 200 kV, obtaining a resolution of 0.14 x 0.25 nm. The X-ray diffraction (XRD) patterns were obtained on a Philips model X`Pert PDP3040 device with Cu Kα1 source (λ = 1.5462 Å), working at 40 kV and 40 mA, with curved single crystal monochromator of copper for eliminating the contributions of Kα2 radiation. The analysis of the diffraction patterns was realized with X`Pert High Score Plus PANalytical database software (version 2.0) (Nutescu Duduman et al., 2016).

2.2. Photocatalytic activity

The photocatalytic degradation was performed in a cylinder shape glass reactor (Fig. 1), equipped with a central quartz tube to host an Osram lamp of 9W and magnetic stirring. The pH value was measured by a Hanna HI 991003 pH-meter and set to the chosen value by adding nitric acid 0.1 M or sodium hydroxide 0.1 M. Prior to the photocatalytic run, the photocatalyst powder finely crushed in a mortar was dispersed in the dye solution, stirred for 30 minutes in dark at room temperature, to reach the adsorption/desorption equilibrium, then the UV lamp was turned on. The time zero concerning the behavior of the dye corresponds to the switch on of the lamp, therefore, the moment when the solid is contacted with the solution means – 30 minutes. Samples of approximately 5 mL mixture were withdrawn at defined time durations from the photo-reactor, filtered through 0.45 μm syringe filter to separate the solid and measured by spectrophotometry.

All experiments were run at ambient temperatures. Rhodamine 6G (R6G) and Methyl Blue (MB) were used as test dyes to evaluate the photocatalytic potential of the solids. The dye concentration were measured by UV–Vis spectroscopy on a Shimadzu UV-1700 spectrophotometer, on the basis of the main maxima of absorption in the visible region of the spectra, situated at 526.5 nm (R6G) and 568 nm (MB), respectively.

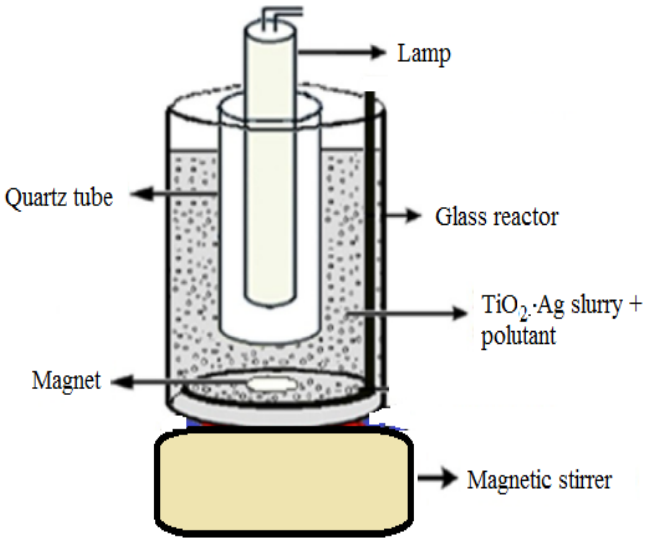

Fig. 1. Experimental setup for photocatalytic tests

The Lambert-Beer law is valid for R6G at concentrations below 12 ppm, therefore the dilution of the solutions of higher concentrations was made accordingly. The conversion degree of the dye was calculated as its decolorization yield, by measuring the concentrations values of the dye by spectrophotometry, using the (Eq. 1):

$$Decolorization\ (\%) = 100\ (C_0 - C)/C_0, \%\qquad (1)$$

where: C_0 is the initial concentration and C is the concentration at time t.

3. Results and discussion

3.1. Sample characterization

The nature of the phases and the crystallinity degree was analyzed by XRD, the patterns are shown in Fig. 2. The peak locations and relative intensities were fitted from the Joint Committee on Powder Diffraction Standards (JCPDS) database: TiO_2anatase (JCPDS 21-1272), TiO_2 rutile (JCPDS 21-1276), silver (JCPDS 04–0783) and silver oxide Ag_2O (JCPDS 00-076-139).

In all samples, the main peaks can be assigned to anatase by the following planes and corresponding 2θ angles: [101] (25.3º); [004] (38º); [200] (48º); [105] (54º); [204] (62.55º) and [116] (69º) (Sakurai and Mizusawa, 2010). The undoped TiO_2 is almost pure anatase, but the noisy pattern suggests the presence of significant amounts of amorphous phase. The larger width and the less sharpness of the peaks of sample S1 compared to S2 indicate that the first sample is less crystalline and has smaller particle size than the other. Also, S1 contains mostly anatase crystalline phase, while S2 is a mixture of anatase and rutile, as proved by the distinctive peaks at 27.5 and 36º, due to the rutile [110] and [101] planes. The lower position of the baseline for sample S2 indicates its higher crystallinity degree compared to S1. Silver was identified in S1 and S2, respectively, as metallic Ag by the peaks at 38.1° [111], 44.5° [200] and 64.4° [220] (Amin et al., 2009; Brook et al., 2007), as AgO (32.8, 34, 38.2 and 40º) and as Ag_2O (38 and 44.5º) (Waterhouse et al., 2001). There are several overlapped peaks between silver and titania, therefore the individual contributions of the mentioned phases were labeled on Fig. 2. The unidentified peaks from S2 marked with asterisk (*) can be assigned to stable silver-organic combinations formed and stabilized during the thermal treatment (Gauri et al., 2016).

The SEM images and an exemplification of EDAX image for the as-synthesized and calcined samples are presented in Fig. 3. Sample S1 consists of compact agglomerations of small, irregularly shaped particles. The calcined sample S2 has a quite similar aspect, even more compact, with some small particles attached on the outer surface of the aggregates.

The EDAX analysis results (Table 2) show that upon calcination, the silver ratio at the surface decreases, indicating its migration inside the titania structure, as previously mentioned in literature (Amin et al., 2009; Hussain et al., 2016; Zhao and Chen, 2011).

Table 2. Elemental composition of samples S1 and S2

Element	***Sample 1***	***Sample 2***
O	51.78±1.2	51.53±1.45
Ti	41.29±0.5	44.29±0.9
Ag	6.94±0.85	4.17±0.4

The high resolution SEM images of samples S1 and S2 are presented in Fig. 4. The structure contains in both cases agglomerated nanoparticles, but their aspect changed significantly after the thermal exposure. In the case of as-synthesized sample, the surface is rather smooth, while during the calcination, the surface becomes rough and has the aspect of agglomerated small flakes.

The TEM and SAED images of samples S1 and S2 are shown in Fig. 5. The TEM images prove the uniform dispersion of the Ag nanoparticles, appearing as dark spots on the major TiO_2 phase. The crystallite size of TiO_2 increases after calcination.

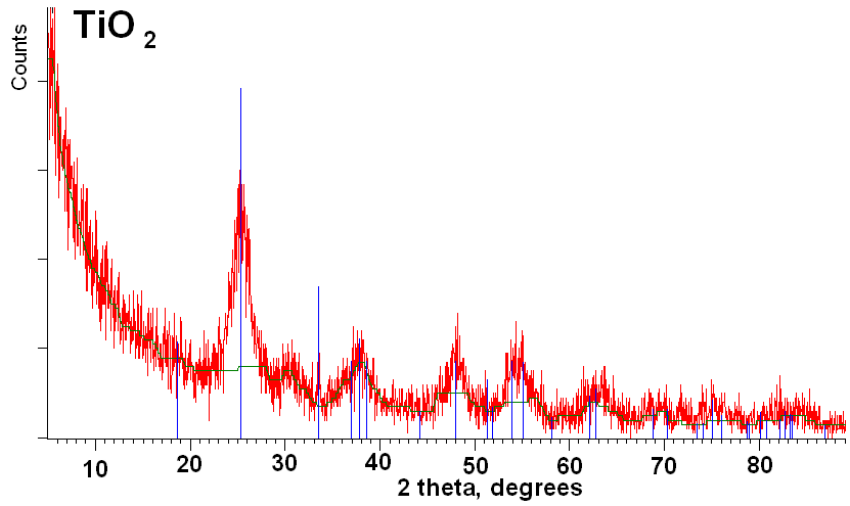

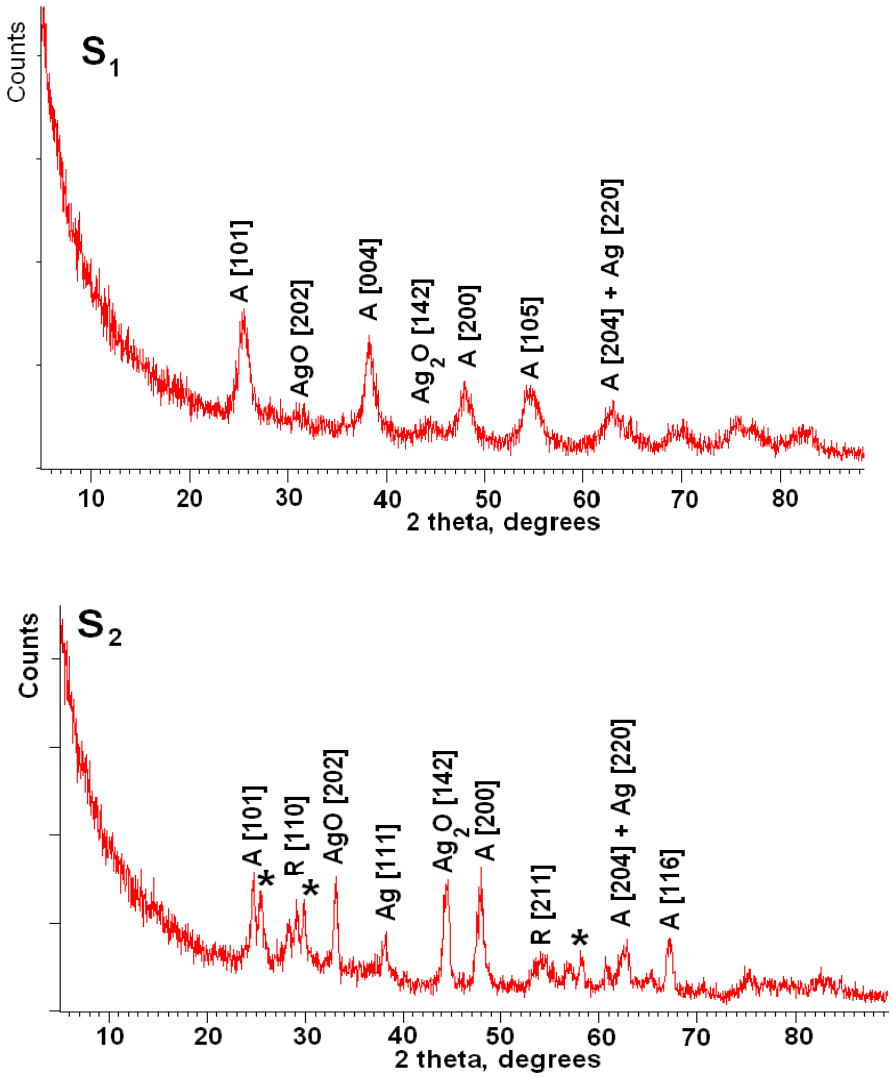

Fig. 2. Powder XRD patterns of synthetized samples: A – anatase, R – rutile

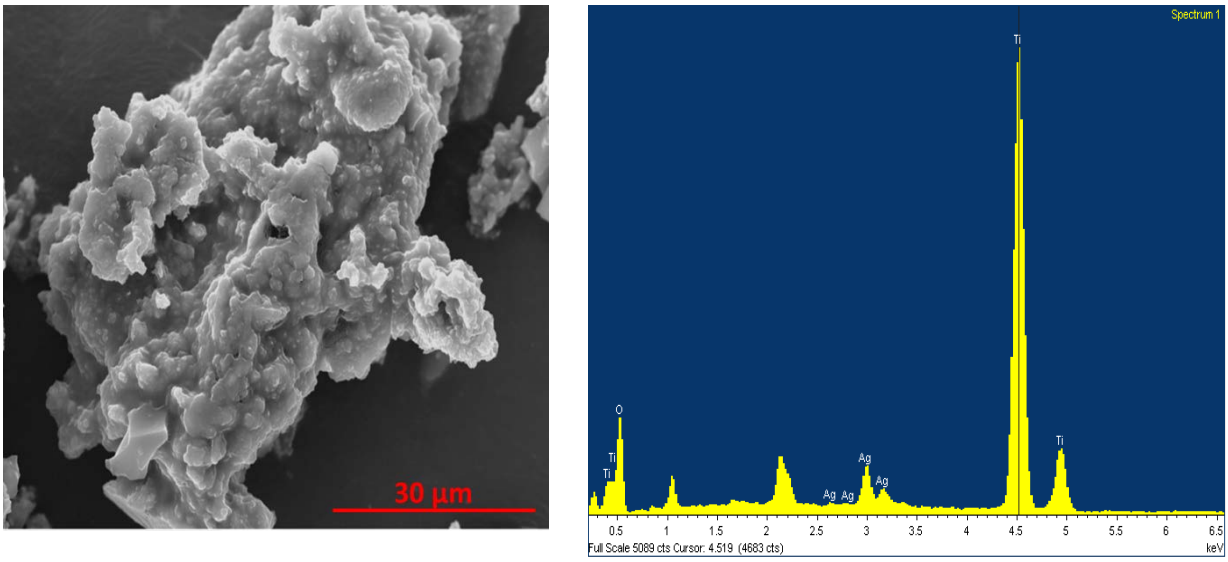

a - S1

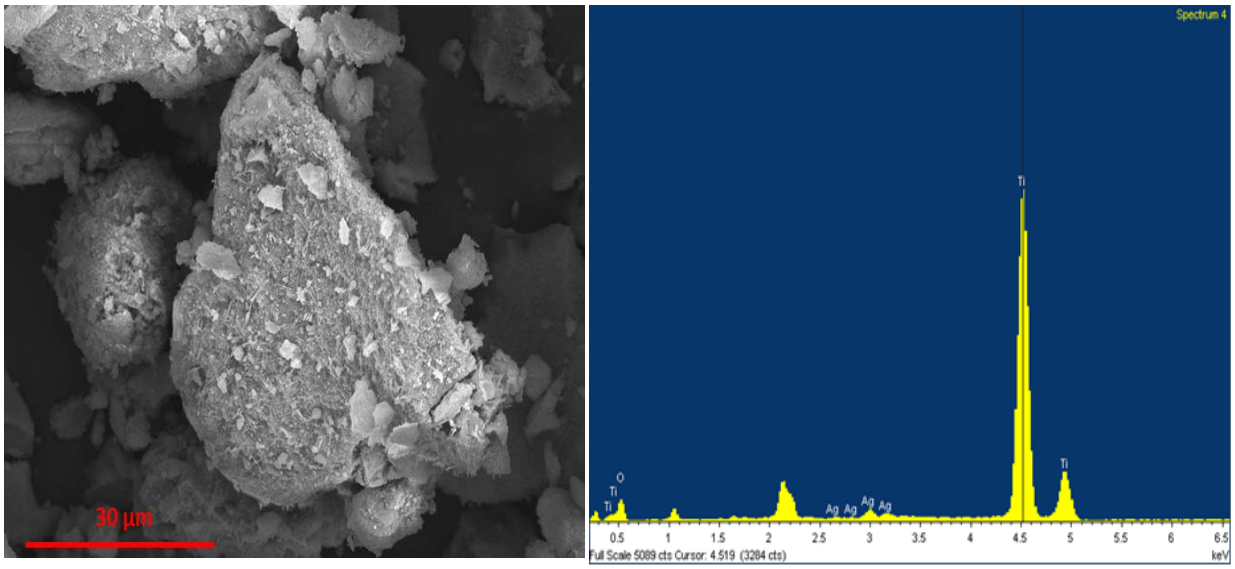

b – S2

Fig. 3. SEM micrographs and EDAX snapshots of samples S1 and S2

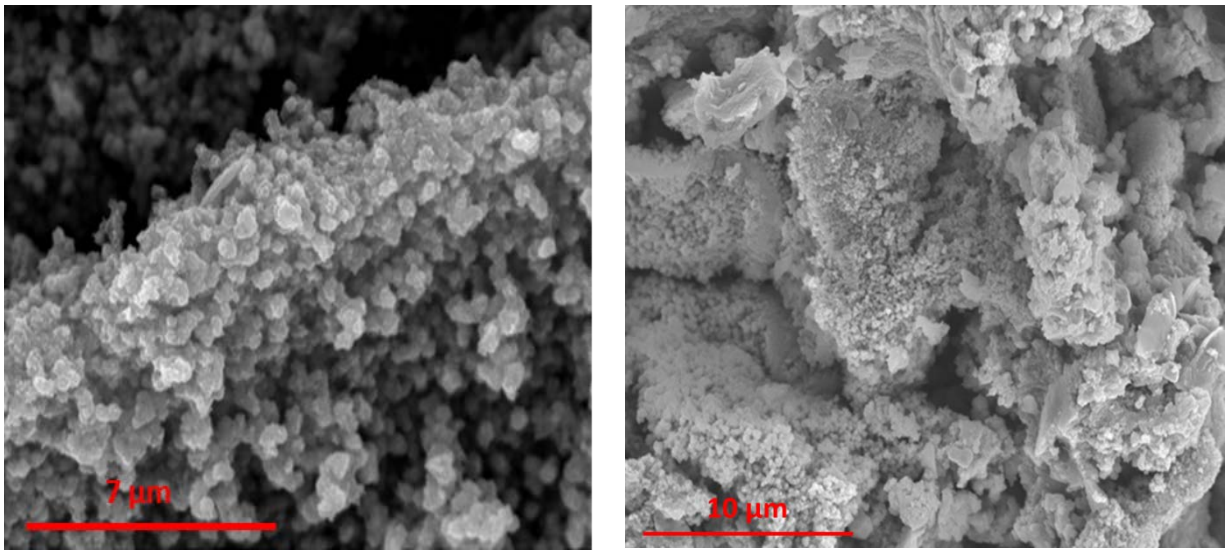

Fig. 4. Micrographs of samples S1 and S2 at high-resolution

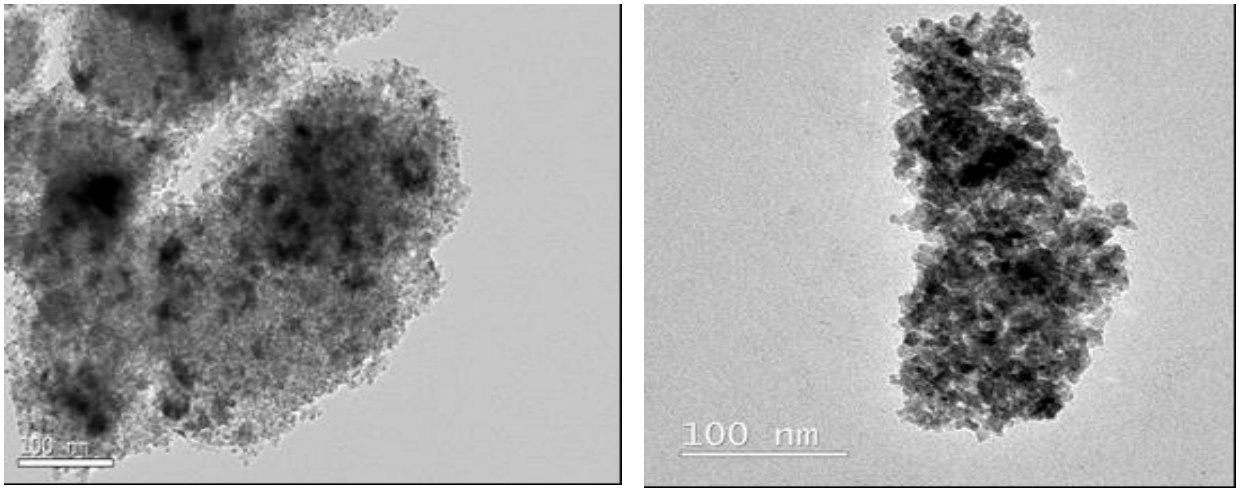

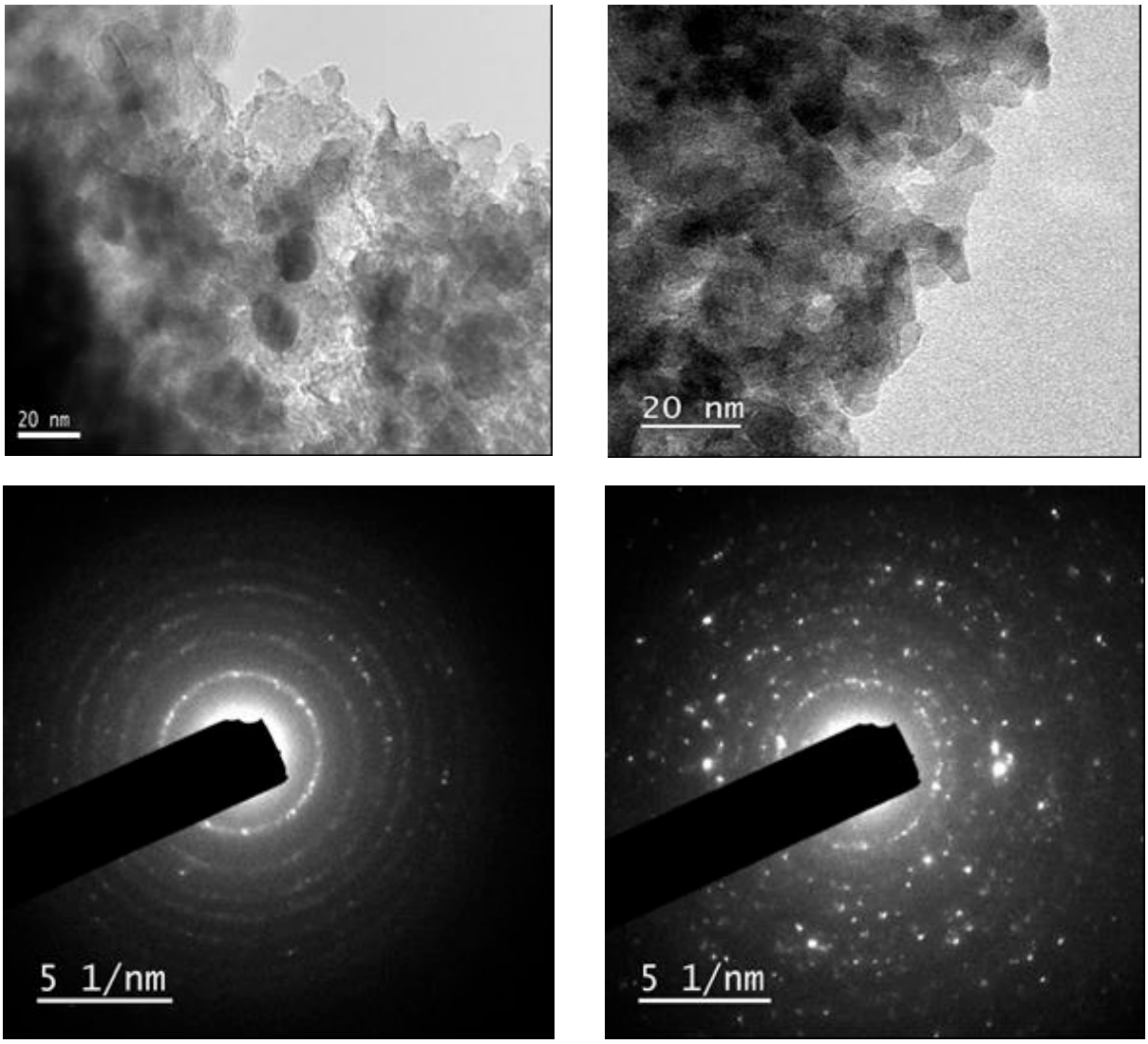

A B

Fig. 5. TEM and SAED of samples S1 (A) and S2 (B)

Table 3. Interplanar distances (Å) for the nanoparticles of S1, deduced from SAED and XRD

Distance from SAED	3.525	2.363	1.90	1.66	1.458
Distance from XRD	3.517	2.366	1.893	1.696	1.483
Interplanar distance from literature (Massard)	3.51	2.33	1.89	1.66	-
Miller indices	[101]	[004]	[200]	[105]	[204]

The SAED pattern of S1 indicates that the crystallinity degree of the samples is not very high, since the rings are not continuous and bright, in line with the results from XRD. After the calcination, the sample becomes poly-nanocrystalline, as shown by the high number of light spots in Fig. 5B.

The SAED image of sample S1 was used to determine the values of the interplanar distances from the structure (Table 3). These values were compared with the theoretically calculated values available in literature (Massard at al, 2012) and the ones obtained from the XRD patterns using the relation of Bragg (Eq. 2):

$$\lambda = 2\,D \sin\theta \qquad (2)$$

where λ is the wavelenght of X-Ray (1.5406 Å), D is the interplanar distance and θ the incidence angle.

The values from Table 3 corelate very well between the two analysis methods and are in agreement with literature data. The investigated area contained only TiO_2-anatase.

3.2. Environmental application

The heterogeneous photocatalytic degradation of organic dyes by TiO_2 and TiO_2-Ag nanocomposites was investigated in the photocatalytic degradation of Rhodamine 6 G (R6G) and Methyl Blue (MB) dyes.

The R6G concentrations were of 15 and 30 ppm, the photocatalyst dose of 1 g L^{-1} and the pH was 4.2 (native value of the dye). In order to improve the

conductivity of the dye solution, a similar experiment was performed using sodium nitrate as an agent to introduce some extra ions in the reaction medium (Atitar et al., 2015).

A comparison between the two series of tests (15 and 30 ppm of dye), in terms of decolorization extent, performed on TiO_2, S1 and S2 of dye is displayed in Fig. 6. The results highlight the beneficial role of Ag doping of the TiO_2 sample. Both S1 and S2 samples have higher photocatalytic activities than the undoped sample, for both dye concentration values. The calcined form has a much better behavior, especially when the dye concentration is low, being able to decompose 85% of the dye in two hours of exposure to UV light from the 15 ppm solution and, respectively, 53% in the case of 30 ppm solution.

The higher activity of the doped titania samples compared with the pure TiO_2 can be explained by the contribution of the silver compounds (Jiang et al., 2015), which have a very low band gap (1.3 eV) and form boundaries by the aggregation of Ag_2O nanoparticles on the support, very efficient in escaping the photogenerated electrons and avoid the recombination electron-hole. On another part, the calcination generates a proper ratio between anatase and rutile (Dariani et al., 2016; Dorian et al., 2011; Ghazzal et al., 2012), which has an important role in the optimization of the electron-hole pair formation and avoiding the recombination process. The position of the energy levels of the valence band and conduction bands of the two phases favors the migration of the promoted electron from the anatase conduction band to the conduction band of rutile, instead allowing the recombination (Scanlon et al., 2013).

An example of the spectra evolution in time (Fig. 7) shows that the decrease of the main peak of R6G from 526.5 nm is strong, as well as that of the peak at 248 nm. Another peak increases progressively around 220 nm, due probably to nitrate ions issued during the degradation of the dye.

The photocatalytic reactions are usually strongly influenced by the pH value and by the conductivity of the solution. A test was made at 30 ppm of R6G at pH of 8 (Lutic and Cretescu, 2016). Some studies (Atitar et al., 2015) indicate that the increase the conductivity of the dye solution is beneficial on the organic compounds removal from solutions. In order to check this fact in our case, a similar experiment was performed using sodium nitrate (0.1 M) as an ions provider in the reaction medium. The decolorization of the dye in time is displayed in Fig. 8.

The results are highly similar in both cases, either using or not the sodium nitrate. The value of the initial solution conductivity did not influence the dye degradation efficiency. The decolorizing degree is of only 34% after 120 minutes and 41% after 180 minutes. So, in our case, the increase of conductivity did not bring any special progress of the decomposition reaction.

The MB dye was also tested as standard compound in the photodegradation. In this case, the initial value of the dye concentration was of 100 ppm and the photocatalyst dose of 0.2 g L^{-1}. The lower solid dose and higher dye concentration chosen are due to the very high efficiency of the photocatalyst in the decolorization. In Fig. 9 is displayed the evolution in time of the MB spectra and in the inset, the evolution in time of the dye concentration.

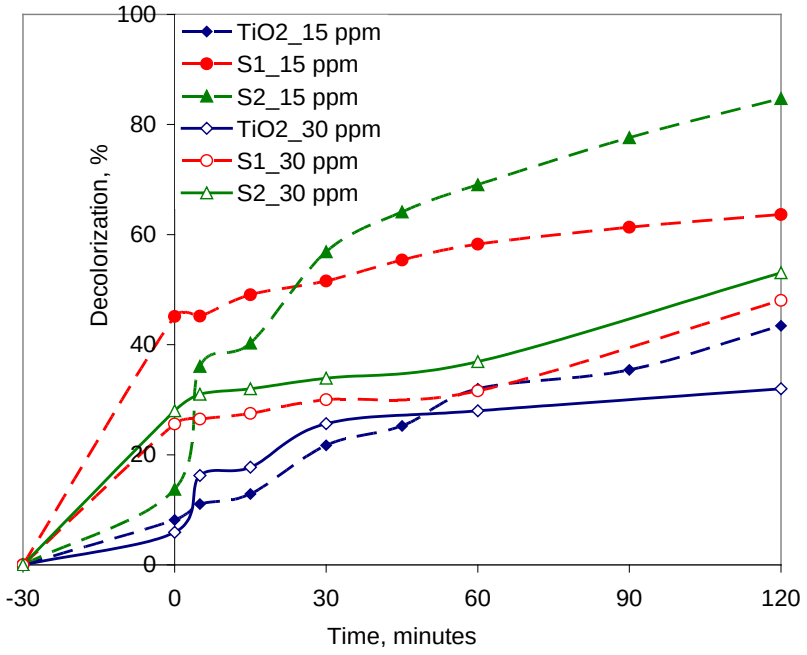

Fig. 6. Conversion versus time of the R6G by photocatalytic degradation on TiO_2-based samples (native dye pH, 1 g L^{-1} photocatalyst dose)

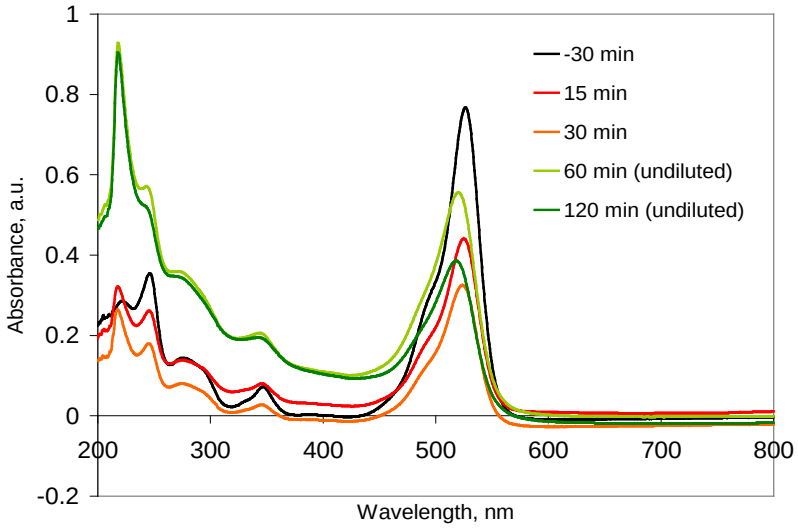

Fig. 7. Spectra evolution in time for 15 ppm of R6G decomposition on S2 (up to 60 min of photocatalysis the dye solution was diluted prior to measuring)

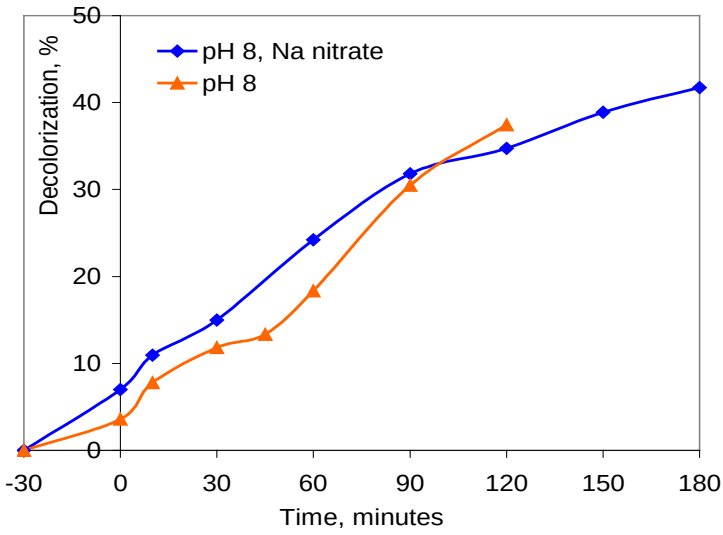

Fig. 8. Influence of sodium nitrate in the reaction medium at pH 8
(1 g L^{-1}photocatalyst dose, 30 ppm R6G initial concentration; 0.1 mol L^{-1} $NaNO_3$)

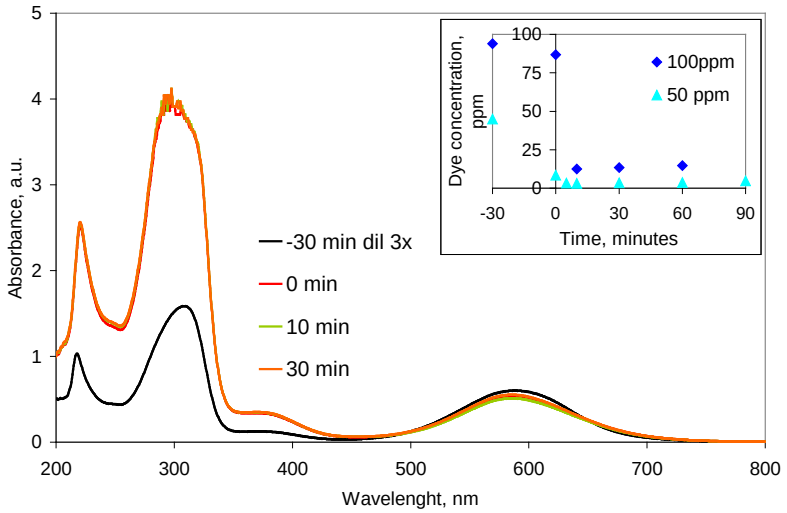

Fig. 9. Spectra in time during the photocatalytic conversion of MB dye (100 ppm MB, 0.2 g L^{-1} solid) and dye concentrations during 120 min of reaction at 100 and 50 ppm of dye

The decomposition of MB is rapid after switching on the UV light. The decolorization is very fast, but only chromophore group is clearly affected in the process. The spectra provide the production of very large and intense peaks in the UV region of the spectrum, indicating that the initial molecule is only splitted in several fragments, not mineralized, as most photocatalytic reactions aim as the target in the environmental applications.

From these two examples, we can conclude that the structure of the dye is of prime importance in evaluating the behavior of the TiO_2-Ag nanocomposites. Despite the activity in the decomposition of R6G is remarkably high only at low dye concentrations, we should be aware of the antiseptic-desinfection potential of silver in real wastewaters treatment and consider this type of solids as interesting to investigate further.

4. Conclusions

The synthesis of a new photocatalyst with disinfection potential, based on Ag-doped TiO_2 nanoparticles was described. The sol-gel method was combined with impregnation-reduction, in order to obtain a good dispersion of the dopant as small nanoparticles on the surface of the majority phase.

Titanium tetra-isopropoxide was used as a TiO_2 precursor in the synthesis: hydrolyzed in nitric acid solution and precipitated by ammonia solution. The obtained solid was then doped with silver nitrate and the ions reduced to silver with hydrazine. The comparison in terms of structural investigation and photocatalytic testing was made between the as-synthesized product and the one obtained by calcination at 650^{o}C.

The characterization of the prepared samples (simple or calcined) was performed by XRD, SEM, TEM and EDAX. The anatase phase was the main component of the as-synthesized product, while a mixture anatase-rutile was detected in the calcined phase. Silver is well dispersed as nanoparticles in the as-synthesized product, while a mixture of Ag, AgO and Ag_2O exists in the calcined product. Also, a migration of Ag inside the structure during the calcination was highlighted by EDAX.

The photocatalytic activity in the decolorizing of R6G dye indicates the beneficial roles of silver as a dopant and of the calcination process. The conversion degree of R6G (15 ppm aqueous solution) on undoped TiO_2 was only 42%, and reached 48% on the as-synthesized sample and respectively 84% on the calcined one. The attempt to enhance the reaction yield by changing the pH value and the conductivity of the reaction medium did not bring any further success.

The MB was decolorized almost totally in 10 minutes, at higher initial concentrations dye values (100 ppm) and lower photocatalyst dose (0.2 g L^{-1}). However, high amounts of organic intermediates absorbing in the UV region of the spectra were produced in the solution, making unattractive an eventual application.

The high decomposition yield of organic dyes and the well-known disinfection potential of Ag-containing solids recommend them for testing in wastewaters needing complex treatments.

Acknowledgements

The authors are grateful for the partial support of this work by the Ministry of Economy and Competitiveness from Spain, Reference: MAT2013-46755-R, and grant POSDRU/159/1.5/S/133652.

References

Amin A.S., Pazouki M., Hosseinnia A., (2009), Synthesis of TiO_2-Ag nanocomposite with sol-gel method and investigation of its antibacterial activity against *E. coli*, *Powder Technology*, **196**, 241-245.

Atitar M.F., Ismail A.A., Al-Sayari S.A., Bahnemann D., Afanasev D., Emeline A.V., (2015), Mesoporous TiO_2nanocrystals as efficient photocatalysts: Impact of calcination temperature and phase transformation on photocatalytic performance, *Chemical Engineering Journal*, **264**, 417-424.

Behnajady M., Bimeghdar S., Eskandarloo H., Photocatalytic activity of Ag/TiO_2–P25-modified cement: optimization using Taguchi approach (2018), *Environmental Engineering and Management Journal*, in press.

Bhakya S., Muthukrishnan S., Sukumaran M., Muthukumar M., Senthil Kumar T., Rao M.V., (2015), Catalytic degradation of organic dyes using synthesized silver nanoparticles: a green approach, *Journal of Bioremediation & Biodegradation*, **6**, 1-9.

Brook L.A., Evans P., Foster H.A., Pemble M.E., Steele A., Sheel D.W., Yates H.M., (2007), Highly bioactive silver and silver/titania composite films grown by chemical vapour deposition, *Journal of Photochemistry and Photobiology A: Chemistry*, **187**, 53-63.

Chen C., Ma W., Zhao J., (2010), Semiconductor-mediated photodegradation of pollutants under visible-light irradiation, *Chemical Society Reviews*, **39**, 4206-4219.

Cheriyan A.J., Shaik F., Baawain A., Said M., Sarkar J.P., (2017), A study on the removal of contaminants from secondary treated municipal wastewater by solar photocatalysis, *Environmental Engineering and Management Journal*, **16**, 1451-1456.

Ciobanu G., Harja M., Rusu L., Mocanu A.M., Luca C., (2014), Acid Black 172 dye adsorption rom aqueous solution by hydroxyapatite as low-cost adsorbent, *Korean Journal of Chemical Engineering*, **31**, 1021-1027.

Ciobanu G., Ilisei S., Harja M., Luca C., (2013), Removal of Reactive Blue 204 dye from aqueous solutions by adsorption onto nanohydroxyapatite, *Science of Advanced Materials*, **5**, 1090-1096.

Dariani R.S., Esmaeili A., Mortezaali A., Dehghanpour S., (2016), Photocatalytic reaction and degradation of methylene blue on TiO_2nano-sized particles, *Optik - International Journal for Light and Electron Optics*, **127**, 7143-7154.

Djoki V.R., Marinkovic A.D., Mitric M., Uskokovic P.S., Petrovic R.D., Radmilovic V.R., Janackovic D.T., (2012), Preparation of TiO_2/carbon nanotubes photocatalysts: the influence of the method of oxidation

of the carbon nanotubes on the photocatalytic activity of the nanocomposites, *Ceramics International*, **38**, 6123-6129.

Dorian A.H., Hanaor D.A.H., Sorrell C.C., (2011), Review of the anatase to rutile phase transformation, *Journal of Materials Science*, **46**, 855-874.

Favier L., Harja M., Simion A.I., Rusu L., Kadmi Y., Pacala M.L., Bouzaza A., (2016), Advanced oxidation process for the removal of chlorinated phenols in aqueous suspensions, *Journal of Environmental Protection and Ecology*, **17**, 1132-1141.

Galkina O.L., Vinogradov V.V., Agafonov A.V., Vinogrado A.V., (2011), Surfactant-assisted sol-gel synthesis of tio2 with uniform particle size distribution, *International Journal of Inorganic Chemistry*, **2011**, 1-8, Article ID 108087.

Gauri B., Vidya K., Dagade S.P., Shobha W., (2016), Synthesis and characterization of Ag/AgO nanoparticles as alcohol sensor, *Research Journal of Chemistry and Environment*, **20**, 1-5.

Ghazzal M.N., Kebaili H., Joseph M., Debecker D.P., Eloy P., De Coninck J., Gaigneaux E.M., (2012), Photocatalytic degradation of Rhodamine 6G on mesoporous titania films: Combined effect of texture and dye aggregation forms, *Applied Catalysis B: Environmental*, **115-116**, 276-284.

Gómez de Salazar J.M., Nutescu Duduman C., Juárez Gonzalez M., Palamarciuc I., Barrena Pérez M. I., Carcea I., (2016), Research of obtaining TiO_2 by sol-gel method using titanium isopropoxide TIP and tetra-n-butyl orthotitanate TNB, *IOP Conference Series: Materials Science and Engineering*, *145, Micro and Nano Technologies*, 1-6.

Hanaor A.H., Sorrell C.C., (2011), Review of the anatase to rutile phase transformation, *Journal of Materials Science*, **46**, 855-874.

Harja M., Barbuta M., Rusu L., Munteanu C., Buema G., Doniga E., (2011), Simultaneous removal of Astrazone blue and lead onto low cost adsorbents based on power plant ash, *Environmental Engineering and Management Journal*, **10**, 341-347.

Harja M., Ciobanu G., Favier L., Bulgariu L., Rusu L., (2016), Adsorption of crystal violet dye onto modified ash, *The Bulletin of the Polytechnic Institute from Iaşi. Chemistry and Chemical Engineering Section*, **62**, 27-37.

He F., Fang Ma, Li J., Li T., Li G., (2014), Effect of calcination temperature on the structural properties and photocatalytic activities of solvothermal synthesized TiO_2 hollow nanoparticles, *Ceramics International*, **40**, 6441-6446.

He Y., Basnet P., Murph S.E.H., Zhao Y., (2013), Ag nanoparticle embedded TiO_2 composite nanorod arrays fabricated by oblique angle deposition: toward plasmonicphotocatalysis, *ACS Applied Materials & Interfaces*, **5**, 11818-11827.

Hu J., Cao Y., Wang K., Jia D., (2017), Green solid-state synthesis and photocatalytic hydrogen production activity of anatase TiO_2 nanoplates with super heat-stability, *RSC Advances*, **7**, 11827-11833.

Hussain M., Tariq S., Ahmad M., Sun H., Maaz K., Ali G., Zahid Hussain S., Iqbal M., Karim S., Nisar A., (2016), Ag-TiO_2nanocomposite for environmental and sensing applications, *Materials Chemistry and Physics*, **181**, 194-203.

Ibrahim A., Mekprasart W., Pecharapa W., (2017), Anatase/Rutile TiO_2 composite prepared via sonochemical process and their photocatalytic activity, *Materials Today: Proceedings*, **4**, 6159-6165.

Ivanova T., Harizanova A., Koutzarova T., Vertruyen B., (2013), Optical and structural characterization of TiO_2 films doped with silver nanoparticles obtained by sol-gel method, *Optical Materials*, **36**, 207-213.

Jiang W., Wang X., Wu Z., Yue X., Yuan S., Lu H., Liang B., (2015), Silver oxide as superb and stable photocatalyst under visible and near-infrared light irradiation and its photocatalytic mechanism, *Industrial and Engineering Chemistry Research*, **54**, 832-841.

Kartal O.E., Turhan G.D., (2017), Determination of electrical energy cost of decolorization of C.I. Acid Orange 7 via TiO_2 -assisted photocatalysis under UV illumination in the presence of H_2O_2, *Environmental Engineering and Management Journal*, **16**, 2045-2052.

Kochuveedu S.T., Kim D.P., (2012), Surface-plasmon-induced visible light photocatalytic activity of TiO_2 nanospheres decorated by Au nanoparticles with controlled configuration, *The Journal of Physical Chemistry C*, **116**, 2500-2506.

Lee M.S., Hong S.S., Mohseni M., (2005), Synthesis of photocatalytic nanosized TiO_2–Ag particles with sol–gel method using reduction agent, *Journal of Molecular Catalysis A: Chemical*, **242**, 135-140.

Liu S.X., Qu Z.P., Han X.W., Sun C.L., (2004), A mechanism for enhanced photocatalytic activity of silver-loaded titanium dioxide, *Catalysis Today*, **93**, 877-884.

Liu X., Bi Y., (2017), In situ preparation of oxygen-deficient TiO_2 microspheres with modified {001} facets for enhanced photocatalytic activity, *RSC Advances*, **7**, 9902-9907.

Liu R., Ren F., Su W., He P., Shen C., Zhang L., Wang C., (2015), Synthesis of TiO_2 hollow spheres with tunable pore structure and enhanced photocatalytic activity, *Ceramics International*, **41**, 14615-14620.

Lutic D., Cretescu I., (2016), Optimization study of Rhodamine 6G removal from aqueous solutions by photocatalytic oxidation, *Revista de Chimie (Bucharest)*, **67**, 134-138.

Lutic D., Coromelci-Pastravanu C., Cretescu I., Poulios I., Stan C.D., (2012), Photocatalytic treatment of Rhodamine 6G in wastewater using photoactive ZnO, *International Journal of Photoenergy*, **2012**, 1-8.

Lutic D., Coromelci C.G., Juzsakova T., Cretescu I., (2017), New mesoporous titanium oxide-based photoactive materials for the removal of dyes from wastewaters, *Environmental Engineering and Management Journal*, **6**, 801-807.

Mahmoodi N.M., Khari F.A., Khatibzadeh M., Gharanjig K., (2017), Synthesis of alginate amide composite using microwave and its dye removal ability, *Environmental Engineering and Management* Journal, **16**, 1859-1866.

Massard C., Bourdeaux D., Raspal V., Feschet-Chassot E., Sibaud Y., Caudron E., Devers T., Awitor K.O., (2012), One-pot synthesis of TiO_2 nanoparticles in suspensions for quantification of titanium debris release in biological liquids, *Advances in Nanoparticles*, **1**, 86-94.

Montazerozohori M., Hoseinipour S.A., (2017), Decolorization of p-dimethylaminobenzal-rhodanine under photocatalytic process by use of titanium dioxide nanoparticles at various buffer pHs, *Environmental Engineering and Management Journal*, **16**, 1853-1858.

Nakata K., Fujishima A., (2012), TiO_2 photocatalysis design and applications, *Journal of Photochemistry and Photobiology C: Photochemistry Reviews*, **13**, 169-189.

Niu Y., Xing M., Tian B., Zhang J., (2012), Improving the visible light photocatalytic activity of nano-sized titanium dioxide via the synergistic effects between

sulfur doping and sulfation, *Applied Catalysis B: Environmental*, **115-116**, 253-260.

Nutescu Duduman C., Gómez De Salazar J.M., Barrena Pérez M.I., Harja M., Palamarciuc I., Gómez De Castro C., (2016a), Obtained of nanocomposites: Cu, CuO and $Cu(OH)_2$ - CNF by sol-gel method, *International Journal of Modern Manufacturing Technologies*, **VIII**, 13-18.

Nutescu Duduman C., Gómez De Salazar J.M., Barrena Pérez M.I., Carcea I., Palamarciuc I., (2016b), Research on obtaining TiO_2-CNF nanocomposites, *International Journal of Modern Manufacturing Technologies*, **VIII**, 30-34.

Pham T.D., Lee B.K., (2004), Effects of Ag doping on the photocatalytic disinfection of *E. coli* in bioaerosol by Ag–TiO_2/GF under visible light, *Journal of Colloid and Interface Science*, **428**, 24-31.

Rupa V., Manikandan D., Divakar D., Sivakumar T., (2007), Effect of deposition of Ag on TiO_2 nanoparticles on the photodegradation of reactive yellow-17, *Journal of Hazardous Materials*, **147**, 906-913.

Rusu L., Harja M., Simion A.I, Suteu D., Ciobanu G., Favier L., (2014), Removal of astrazone blue from aqueous solutions onto brown peat. Equilibrium and kinetics studies, *Korean Journal of Chemical Engineering*, **31**, 1008-1015.

Sakurai K., Mizusawa M., (2010), X-ray diffraction imaging of anatase and rutile, *Analytical Chemistry*, **82**, 3519-3522.

Sarina S., Waclawik E.R., Zhu H., (2013), Photocatalysis on supported gold and silver nanoparticles under ultraviolet and visible light irradiation, *Green Chemistry*, **15**, 1814-1833.

Scanlon D.O, Dunnill C.W., Buckeridge J., Shevlin S.A., Logsdail A.J., Woodley S.M., Catlow C.R.A., Powell M.J., Palgrave R.G., Parkin I.P., Watson G.W., Keal T.K., Sherwood P., Walsh A., Sokol A.A., (2013), Band alignment of rutile and anatase TiO_2, *Nature Materials*, **12**, 798-801.

Tian B., Dong R., Zhang J., Bao S., Yang F., Zhang J., (2014), Sandwich-structured AgCl@Ag@TiO with excellent visible-light photocatalytic activity for organic pollutant degradation and *E. coli* K12 inactivation, *Applied Catalysis B: Environmental*, **158-159**, 76-84.

Tobaldi D.M., Pullar R.C., Gualtieri A.F., Seabra M.P., Labrincha J.A., (2013), Sol-gel synthesis, characterisation and photocatalytic activity of pure, W, Ag and W/Ag co-doped TiO_2 nanopowders, *Chemical Engineering Journal*, **214**, 364-375.

Vajda K., Saszet K., Kedves E.Z., Kása Z., Danciu V., Baia L., Magyari K, Hernádi K, Kovács G., Pap Z., (2016), Shape-controlled agglomeration of TiO_2 nanoparticles, New insights on polycrystallinity vs. single crystals in photocatalysis, *Ceramics International*, **42**, 3077-3087.

Wang M., Zhang W., Zheng X., Zhu P., (2017), Antibacterial and catalytic activities of biosynthesized silver nanoparticles prepared by using an aqueous extract of green coffee bean as a reducing agent, *RSC Advances*, **7**, 12144-12149.

Waterhouse G.I.N., Bowmaker G.A., Metson J.B., (2001), The thermal decomposition of silver (I, III) oxide: A combined XRD, FT-IR and Raman spectroscopic study, *Physical Chemistry Chemical Physics*, **3**, 3838-3845

Wei P., Liu J., Li Z., (2013), Effect of Pt loading and calcination temperature on the photocatalytic hydrogen production activity of TiO_2 microspheres, *Ceramics International*, **39**, 5387-5391.

Yin H., Yu K., Song C., Huang R., Zhu Z., (2014), Synthesis of Au-Decorated V_2O_5@ZnO heteronanostructures and enhanced plasmonic photocatalytic activity, *ACS Applied Materials & Interfaces*, **6**, 14851-14860.

Zhao B., Chen Y.W., (2011), Ag/TiO_2 sol prepared by a sol-gel method and its photocatalytic activity, *Journal of Physics and Chemistry of Solids*, **72**, 1312-1318.